Supporting Information for "Burying Earth's primitive mantle in the slab graveyard"

T.D. Jones[1,2], N. Sime[1], P.E. van Keken[1]

[1]Earth and Planets Laboratory, Carnegie Institution for Science, Washington, District of Columbia, U.S.A.
[2]Now at Institute of Geophysics and Planetary Physics, University of California San Diego, California, U.S.A.

S1 On the importance of pointwise divergence free velocity field approximation

Our goal in this section is to demonstrate the importance of precise approximation of the mass continuity equation in geodynamics simulations. We show by example that naïve imposition of the mass conservation constraint in the Stokes system may yield qualitatively spurious results. We do this by reproduction of the numerical experiment exhibited in Christensen and Hofmann (1994) and also demonstrated in Brandenburg and van Keken (2007).

We refer to Sime et al. (submitted) for more details regarding so-called divergence free approximation schemes and their importance in tracer advection. Futhermore we refer to Maljaars et al. (in press) for details regarding our computational implementation with the LEoPart library. The code used to generate the results exhibited in this section is available in the repository (Sime, 2020).

S1.1 Numerical experiment

The numerical model is composed as follows, where the physical constants imposed in the system are tabulated in table S1. In the computational rectangle domain $\Omega = (0, 4) \times (0, 1)$ we seek finite element approximations of velocity, pressure and temperature, $\mathbf{u}$, p and T, respectively, in addition to an approximation of composition Γ by tracer data, such that:

$$\frac{\partial T}{\partial t} - \nabla^2 T + \mathbf{u} \cdot \nabla T = Q, \tag{S1}$$

$$-\nabla \cdot \sigma = (\alpha(z)\mathrm{Ra}T - \beta(z)\mathrm{Rb}\Gamma)\hat{\mathbf{k}}, \tag{S2}$$

$$\nabla \cdot \mathbf{u} = 0. \tag{S3}$$

Here t is the simulation time, Ra is the thermal Rayleigh number, Rb is the compositional Rayleigh number, Q is the heat source constant, $\hat{\mathbf{k}} = (0, 1)^\top$ is the buoyancy unit vector and

$$\sigma = 2\eta(T)(\nabla \mathbf{u} + \nabla \mathbf{u}^\top) - pI \tag{S4}$$

is the stress tensor defined in terms of the identity tensor I and viscosity

$$\eta(T) = \eta_0 \exp\left(-b\left(T - \tfrac{1}{2}\right) + c\left(z - \tfrac{1}{2}\right)\right), \tag{S5}$$

where η_0, b and c are constants. Furthermore,

$$\alpha(z) = \frac{d}{1 - e^{-d}} e^{-dz}, \tag{S6}$$

$$\beta(z) = \frac{s}{1 - e^{-s}} e^{-sz}, \tag{S7}$$

$$z = 1 - y, \tag{S8}$$

Corresponding author: T.D. Jones, t6jones@ucsd.edu

where d and s are prescribed constants.

The velocity boundary conditions are imposed as follows:

1. $\tau \cdot (\sigma \cdot n) = 0$ and $\mathbf{u} \cdot \mathbf{n} = 0$ on the bottom, left and right boundaries, $y = 0$, $x = 0$ and $x = 4$, respectively. Here τ is a unit vector lying tangential to the boundary,
2. $\mathbf{u} = (u_{\mathrm{h,top}}, 0)^\top$ on the top boundary $y = 1$.

Here the function u_{top} is prescribed to be

$$u_{\mathrm{top}} = \pm u_0 + \frac{\pi u_0}{10} \sin\left(\frac{\pi u_0}{5} t\right) \tag{S9}$$

where

$$\pm u_0 = \begin{cases} +u_0 & x \leq x_c, \\ -u_0 & x > x_c, \end{cases} \tag{S10}$$

$$x_c = 2 + \cos\left(\frac{\pi u_0}{5} t\right) \tag{S11}$$

and u_0 is a constant. We use a mollified Heaviside function to approximate u_{top} by $u_{\mathrm{h,top}}$ so to satisfy the regularity requirements of conforming finite element methods such that

$$u_{\mathrm{h,top}} = -u_0 \left(\frac{2}{1 + e^{-2k(x - x_c)}} - 1\right) + \frac{\pi u_0}{10} \sin\left(\frac{\pi u_0}{5} t\right), \tag{S12}$$

where k is a constant. Equation (S12) can intuitively be interpreted as a 'smoothing' of the step function equation (S10), see Figure S1 for example.

Constant	Value
Ra	5×10^5
Rb	3.88×10^5
η_0	1
Q	2.5
b	65 536
c	64
s	$\ln 2$
d	$\ln 6$
k	10
u_0	500
x_m	0.08
z_m	0.08
z_c	0.01

Table S1: Physical and mathematical constants employed in the numerical experiment.

S1.2 Melting

Two rectangular melting regions are defined at the top left and top right of the computational domain

$$\Omega_{\mathrm{melt,left}} = (0.0, x_m) \times (1 - z_m, 1 - z_c), \tag{S13}$$

$$\Omega_{\mathrm{melt,right}} = (4 - x_m, 4) \times (1 - z_m, 1 - z_c), \tag{S14}$$

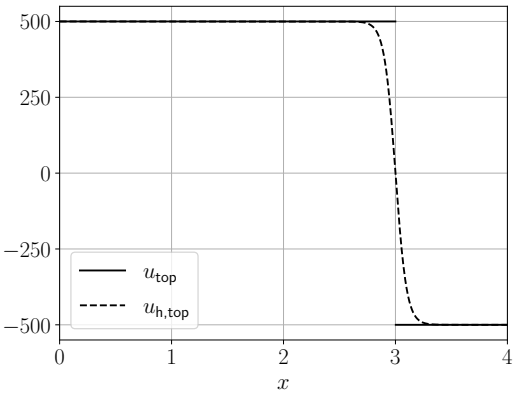

Figure S1: Boundary condition function u_{top} and $u_{\text{h,top}}$ where $k = 10$ at simulation time $t = 0$. The smoothed function $u_{\text{h,top}}$ adheres to the smoothness regularity requirement of standard finite element methods.

where x_m is the width of the melt zones and (z_m, z_c) is the depth interval of the melt zones. Given N_p tracers in the simulation, should a tracer's position $\mathbf{x}_n = (x_n, y_n)^\top$, $n = 1, \ldots, N_p$ enter a melt zone as defined above, its y-coordinate position will be changed such that the tracer now resides in the melted regions

$$\Omega_{\text{melted,left}} = (0.0, x_m) \times (1 - z_c, 1), \tag{S15}$$

$$\Omega_{\text{melted,right}} = (4 - x_m, 4) \times (1 - z_c, 1), \tag{S16}$$

respectively. In essence, those particles in the melt zones have their positions changed according to

$$\mathbf{x}_{n,\text{melted}} = \big(x_n, \mathcal{U}(1 - z_c, 1)\big)^\top \quad \forall \mathbf{x}_n \in \Omega_{\text{melt,left}} \cup \Omega_{\text{melt,right}},\ n = 1, \ldots, N_p. \tag{S17}$$

Here $\mathcal{U}(a, b)$ is a number selected from the uniform random distribution defined on the interval (a, b).

S1.3 Divergence free constraint (pointwise) correction

A key component in modeling incompressible flow is the precise approximation of the continuity constraint equation (S3). Sime et al. (submitted) demonstrates the benefits of pointwise satisfaction of the continuity constraint (referred to as a pointwise divergence free velocity approximation) such that

$$\nabla \cdot \mathbf{u}_h(\mathbf{x}) = 0 \quad \forall \mathbf{x} \in \Omega, \tag{S18}$$

where $\mathbf{u}_h$ is the finite element approximation of the velocity. This is achieved in Sime et al. (submitted) be employing the hybridized discontinuous Galerkin finite element method. However, in this example we will use a Taylor–Hood discretisation scheme and solve for the Stokes system by an iterated penalty method demonstrated in Morgan and Scott (2018). In this setting, although we do not satisfy equation (S18) to machine precision, we achieve a better approximation by orders of magnitude compared with the standard solution obtained by the Taylor–Hood scheme.

In the following results section by 'div-corrected' we refer to the solution scheme by the iterated penalty method (Morgan & Scott, 2018) offering a corrected divergence free field. By '*non* div-corrected' we refer to the standard solution of the Stokes system discretized by Taylor–Hood elements.

S1.4 Results

Tracer distribution snapshots are shown in Figure S2. For direct comparison with Christensen and Hofmann (1994) and Brandenburg and van Keken (2007) we convert the time scale to dimensional time by

$$t' = tu_0\mathcal{T}, \tag{S19}$$

where $\mathcal{T} = 60\,\text{Ma}$ is the characteristic overturn time of the mantle. Clearly we see the formation of piles at the base of the geometry in the div-corrected scheme. In the *non* div-corrected scheme we obtain a qualitatively different result to Christensen and Hofmann (1994) and Brandenburg and van Keken (2007) in which piles do not form. Examining further we plot histograms of depth dependent tracer frequencies in Figure S4. In the *non* div-corrected scheme we see evidence of tracers 'settling' to the base of the geometry.

The rate of accumulation F_s is shown in Figure S3, where

$$\begin{aligned} F_s = {} & \text{the fraction of particles in piles at the core-mantle boundary} \\ & \text{relative to the total number of particles in the model.} \end{aligned} \tag{S20}$$

where piles are quantitatively defined by grid cells that have a particle concentration >30% and are part of a vertically continuous column starting at the CMB. Particle concentration assumes a particle volume Vol_n defined by

$$\text{Vol}_n = \frac{C \times \text{Vol}(\Omega)}{N_p}, \quad n = 1, \ldots, N_p, \tag{S21}$$

where C=0.125 is the fraction of the mantle assumed to be composed of basalt, $\text{Vol}(\Omega) = \int_\Omega \mathrm{d}x$ is the total domain volume and N_p is the total number of particles in the model.

In the div-corrected case we see in Figure S3 that our computed value of F_s compares well with Christensen and Hofmann (1994) and Brandenburg and van Keken (2007), consolidating at around $F_s \approx 0.12$. However, in the *non* div-corrected case, the tracers sinking to the bottom of the geometry yield consistent growth of the F_s curve.

References

Brandenburg, J. P., & van Keken, P. E. (2007). Deep storage of oceanic crust in a vigorously convecting mantle. *Journal of Geophysical Research*, *112*, B06403.

Christensen, U. R., & Hofmann, A. W. (1994). Segregation of subducted oceanic crust in the convecting mantle. *Journal of Geophysical Research*, *99*, 19867–19884.

Maljaars, J. M., Richardson, C. N., & Sime, N. (in press). LEoPart: a particle library for FEniCS. *Computers & Mathematics with Applications*. doi: 10.1016/j.camwa.2020.04.023

Morgan, H., & Scott, L. R. (2018). Towards a unified finite element method for the Stokes equations. *SIAM Journal on Scientific Computing*, *40*(1), A130–A141.

Sime, N. (2020). *GeoPart: Particles in geodynamics supporting code.* `https://bitbucket.org/nate-sime/geopart`.

Sime, N., Maljaars, J. M., Wilson, C. R., & van Keken, P. E. (submitted). An exactly mass conserving and pointwise divergence free velocity method: application to compositional buoyancy driven flow problems in geodynamics. *Submitted to Geochemistry Geophysics Geosystems*.

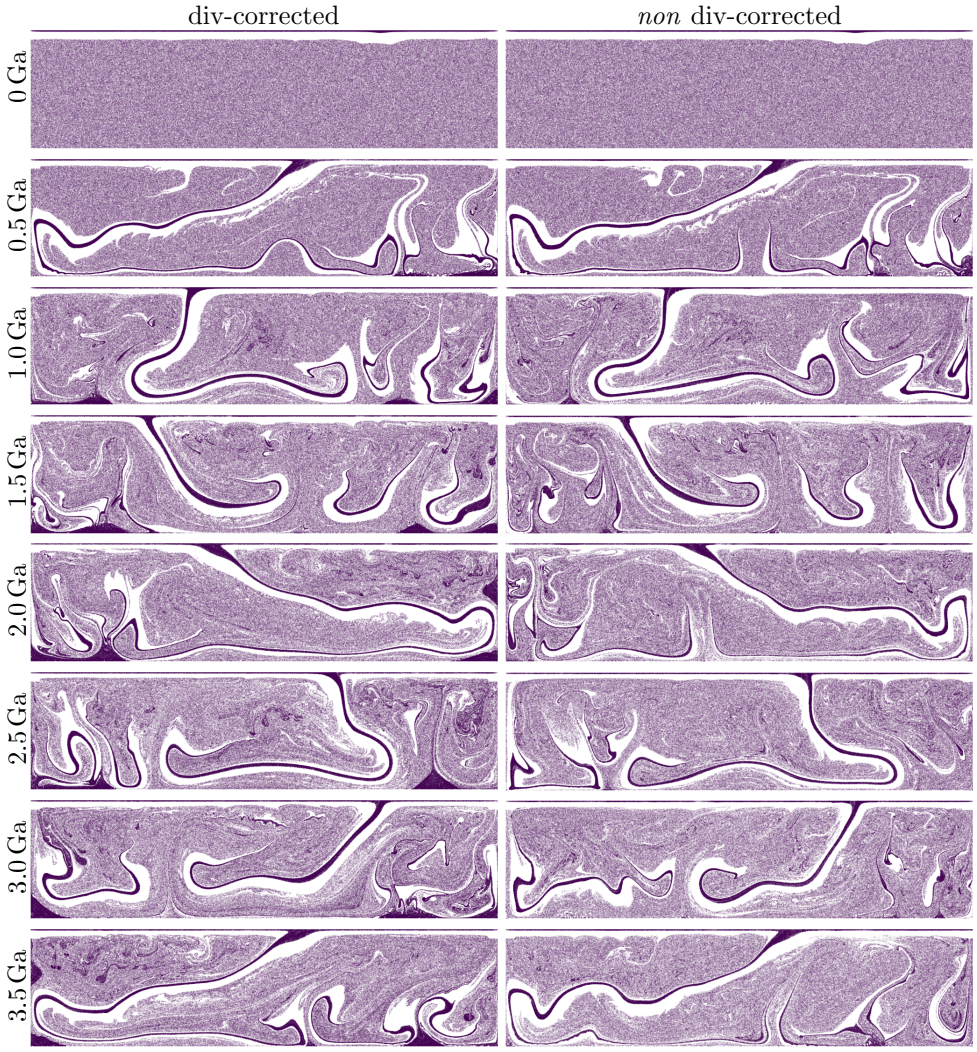

Figure S2: Snapshots of the tracer distribution in the numerical experiment at specified dimensional times t' (see equation (S19)). The left and right columns depict div-corrected and *non* div-corrected simulations, respectively. Note the qualitative appearance of piles only in the simulation where the div-correction has been applied.

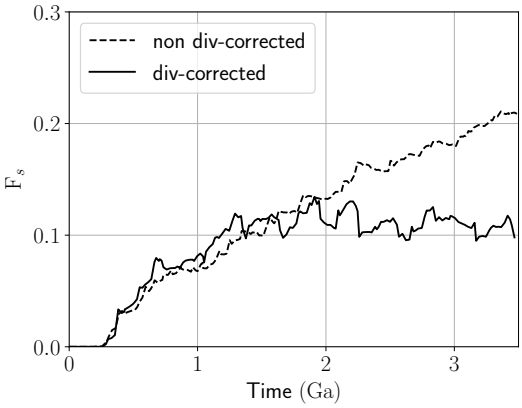

Figure S3: Computed functional F_s measuring the accumuluation of piles. Note that in the *non* div-corrected simulation the tracer settling towards the base of the geometry yields the spurious result of consistent growth in F_s. Employing the div-correction scheme, F_s consolidates around approximately 0.12 (cf. Christensen & Hofmann, 1994; Brandenburg & van Keken, 2007).

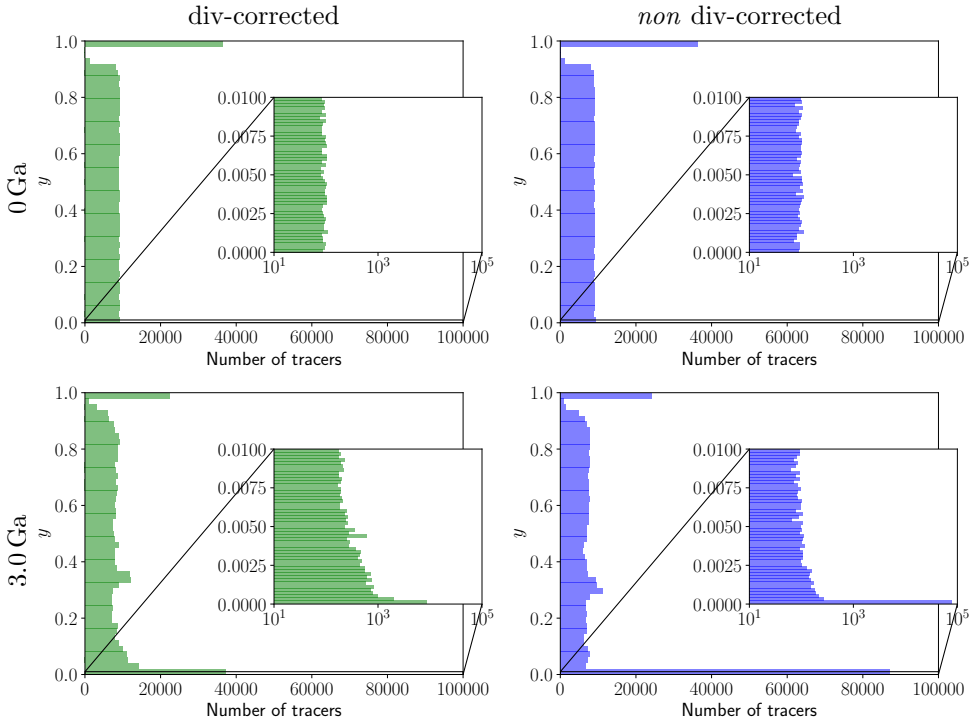

Figure S4: Histograms of tracer frequency with depth y. Note the 'smooth' distribution of tracers in the div-corrected scheme as the simulation evolves. In the *non* div-corrected case, tracers rapidly sink to the base of the geometry. The inset axes show histograms of tracer frequency at the base of the geometry in the depth interval $y \in (0, 0.01)$.